Dynamics of a Puelche foehn event in the Andes

Meteorologische Zeitschrift, Vol. 27, No. 1, 67–80 (published online December 1, 2017)

Dynamics of a Puelche foehn event in the Andes

Lea Beusch[1], Shira Raveh-Rubin[1], Michael Sprenger[1*] and Lukas Papritz[2,1]

[1]ETH Zürich, Institute for Atmospheric and Climate Science, Switzerland
[2]Geophysical Institute, University of Bergen, and Bjerknes Centre for Climate Research, Bergen, Norway

(Manuscript received November 24, 2016; in revised form August 15, 2017; accepted August 15, 2017)

Abstract

In this numerical modelling study, we investigate a Puelche foehn event (25–26 March 2014) in the southern Andes – a region with sparse observations. The synoptic environment as well as the mesoscale structure and the dynamics of the easterly wind are examined with European Centre for Medium-Range Weather Forecasts (ECMWF) analyses and a simulation with the mesoscale non-hydrostatic limited-area weather prediction model COSMO with a grid spacing of 2.2 km.

The large-scale synoptic situation leading to this Puelche event is characterized by a mid-tropospheric cut-off low above the mountain range, the formation of a coastal surface low, as well as high pressure extending over the southern Andes. Easterly winds extend throughout the entire troposphere, indicative of a deep foehn flow. In the free troposphere, the easterlies are geostrophically balanced and develop in association with increasing pressure to the south. In contrast, within the planetary boundary layer, the easterly winds occur predominantly due to an increasing cross-range large-scale pressure gradient with only a weak geostrophic component. Kinematic trajectories indicate that a significant part of the Puelche air mass originates from above an inversion on the upstream side of the Andes. Some air parcels, however, ascend on the upstream side to crest height as the boundary layer deepens during daytime and/or flow through gaps across the mountain range. Hence, this Puelche event shares characteristics of both a blocked and a non-blocked foehn type.

Keywords: Puelche, Andes, foehn mechanisms, downslope flows, COSMO simulation, trajectories

1 Introduction

The Andes Cordillera in the western part of South America extends from ~10° N to ~53° S and has a typical width of less than 200 km. Its mean height decreases rapidly from 35° S southward to a mean level of 1500 m, whereas peaks over 6000 m are common to the north. Due to their meridional extent and height, the Andes significantly influence the atmospheric circulation (Garreaud, 2009). This results in weather phenomena across various spatial and temporal scales (e.g., cold surges on the eastern side of the Andes; Sprenger et al., 2013), as well as distinctly contrasting climate conditions along the eastern and western sides of the mountain range (Hobbs et al., 1998). In particular, foehn or foehn-like flows, defined as strong, warm, and very dry winds descending in the lee of mountains (Brinkmann, 1971), are abundant in the Andes. These winds carry many different names such as Puelche, Terral, Raco, and Zonda, depending on the region where they occur (Montecinos et al., 2017)[1], and they have tremendous societal and environmental impacts. The Puelche, for instance, is known to induce glacier melt (Brock et al., 2012) and cause strong mixing in Lake Villarrica which can result in phytoplankton bloom (Meruane et al., 2006); the Terral affects agriculture (Montes et al., 2016); the Raco is held accountable for severe air pollution events over Santiago (Rutllant and Garreaud, 2004); and the Zonda can be accompanied by destructive wind gusts (Seluchi et al., 2003).

The occurrence of foehn winds is not restricted to the Andes but found all over the world with the most studied examples located in the European Alps (north and south foehn; e.g., Drobinski et al., 2007, and references therein) and the Rocky Mountains in North America (chinook; e.g., Nkemdirim, 1996). Even though this phenomenon is so prevalent and has fascinated humans for centuries (see, e.g., Sprenger et al., 2016, for a history of foehn research in Switzerland; and Kuhn, 1989, for a broader overview of foehn history and research in the European Alps), its underlying mechanisms are still not fully understood. Furthermore, it remains highly challenging to accurately forecast these events (Richner and Hächler, 2013).

In contrast to the foehn winds in the Alps and in the Rocky Mountains, the foehn winds in the Andes have not been extensively studied yet, partly due to the sparse observational network in these regions (Seluchi et al., 2003). Most studies focus on the synoptic conditions leading to foehn events. Rutllant and Garreaud (2004) distinguish three different synoptic and meso-

*Corresponding author: Michael Sprenger, ETH Zürich, Atmospheric and Climate Science, Universitätsstrasse 16, 8092 Zürich, e-mail: michael.sprenger@env.ethz.ch

[1]The easterly Raco and Terral foehn winds are associated with specific valleys: the Raco with the San José de Maipo valley south of Santiago, and the Terral with the Elqui valley near La Serena. The easterly Puelche wind, on the other hand, extends over a region of 600 km in latitude and is not directly associated with a specific valley. The westerly Zonda occurs in west-central Argentina.

DOI 10.1127/metz/2017/0841
Gebrüder Borntraeger Science Publishers, Stuttgart, www.borntraeger-cramer.com

scale settings (categories) associated with Raco foehn winds. Meruane et al. (2006) state that the Puelche foehn typically develops under similar synoptic conditions as two of these Raco categories, and we therefore briefly discuss them. The first Raco category, including about 64 % of all events, is characterized by a surface anticyclone extending from the Pacific Ocean across the Andes in southern Chile, and by a narrow near-surface trough along the coast of Chile (Fig. 6a in Rutllant and Garreaud, 2004). The strong southward pressure gradient between the coastal low and the anticyclone induces an easterly, geostrophically balanced flow across the Andes (Garreaud et al., 2002). According to Montecinos et al. (2017), Raco and Puelche events do, however, not occur simultaneously since the latitudinal position of the anticyclone determines which one of these easterly foehn systems develops. The mid-tropospheric flow (at 500 hPa), is governed by a ridge to the west of the subtropical Andes and a trough to the east, leading to south-westerlies down to about 700 hPa over the mountain range (Rutllant and Garreaud, 2004). Hence, easterly winds are restricted to the lower troposphere (below 700 hPa). In the European Alps, a similar decoupling of low- and mid-tropospheric flow during foehn is referred to as a 'shallow foehn' (Seibert, 1990; Sprenger and Schär, 2001). The second category of Raco events (16 %) is similar to the first category in terms of the near-surface synoptic (anticyclone) and mesoscale (coastal low) setting, but the mid-tropospheric flow differs: The mid-tropospheric ridge tilts in the NW-SE direction, resulting in a cut-off low over the Andes, hence leading to a south-easterly flow across the Andes also at these levels (Rutllant and Garreaud, 2004). Accordingly, this type of foehn classifies as a 'deep foehn' in the terminology used in the European Alps (Seibert, 1990; Sprenger and Schär, 2001).

The synoptic classification of Raco and Puelche can be complemented by a further concept that is well known from the south foehn in the European Alps. During foehn, the near-surface air on the Alpine south side (in the Po valley) can either be blocked or surmount the Alpine ridge (non-blocked). This distinction goes back to one of the first foehn pioneers, Julius von Hann, who called it type I and type II foehn, respectively, and used it to explain the warming of foehn air (Hann, 1866). Over the years, the terminology changed to 'Swiss' and 'Austrian' foehn types, where the former corresponds to the non-blocked and the latter to the blocked flow situation. Wuersch and Sprenger (2015) use a Lagrangian approach to assess the relative frequency of the two foehn types in a Swiss and Austrian valley. They show that Austrian foehns are indeed predominantly, but not exclusively, found in Austria; and vice versa for the Swiss foehn. We can expect that blocked foehn types dominate in parts of the Andes, especially from central Chile northward, where the mountain range is very high with peaks reaching beyond 6000 m. However, the situation is less clear for Puelche winds further south. Montecinos et al. (2017) conclude their study by stating that the "Terral and Raco winds are not linked with upslope movement in the Argentinian slope of the Andes [...]. However, the Puelche wind is part of a zonal circulation from Argentina (upslope) to Chile (downslope) [...]". Hence, the Raco might be similar to the blocked foehn type, whereas the Puelche might show characteristics of both, blocked and non-blocked foehn types.

Rutllant and Garreaud (2004) argue that the across-Andes flow during Raco in central Chile (~ 33° S) cannot be explained by the strong cross-range gradients in near-surface geopotential height because of the high mountain altitudes. In fact, they show that the strong zonal gradients in geopotential height are confined to levels below 3000 m, whereas the lowest across-Andes gaps are at a height of about 3500 m. This is in contrast to other foehn winds, e.g., in the Washington Cascade Mountains (Colle and Mass, 1998), where exactly these gradients play a crucial role in driving the cross-mountain flow. Accordingly, Rutllant and Garreaud (2004) conclude that the across-mountain wind must be predominantly geostrophically balanced. For the Puelche, the situation is again less clear. The mountains in the Puelche's region south of 35° S drop from 4000 m to below 2000 m, and therefore "it is expected that the easterly winds flowing across the Andes from Argentina (upslope) to Chile (downslope) may be forced by both zonal and meridional pressure gradients" (Montecinos et al., 2017). In the same study, this effect is quantified based on a reanalysis dataset (from 1979 to 2015) of 0.5° × 0.5° grid spacing. To this aim, the *zonal* wind component (as an indicator for Puelche winds) is correlated with the *meridional* and *zonal* near-surface pressure gradients – the former gradient indicating a geostrophic across-mountain flow, and the latter gradient indicating a cross-range-pressure-driven across-mountain flow. A strong anti-correlation exceeding −0.7 between the *zonal* pressure gradient and the *zonal* wind, is found south of 35° S on the western slopes of the Andes pointing towards the importance of the ageostrophic cross-range flow. At these latitudes, also a positive correlation between the *meridional* pressure gradient and the *zonal* wind is observed, indicating that the flow is partly driven by the geostrophic balance. Thereby, the strongest correlation (exceeding 0.7) is found south of 37° S, where the crest height is below 2000 m.

Of course, one might wonder whether it is acceptable to restrict the Puelche driving mechanisms to meridional and zonal large-scale pressure gradients? The question is justified, given the large list of further processes that have been found to be important for the dynamics of, e.g., the Alpine foehn. Among these ingredients we only list a few (for further processes, please consider the references in the following articles): (i) gravity waves (Drobinski et al., 2007); (ii) gap flows (Mayr et al., 2007); (iii) transitions from sub- to supercritical flows (Durran, 1990; Gohm and Mayr, 2004); (iv) wave breaking and critical levels (Klemp and Lilly, 1975);

(v) inversion layers on the upstream side (Gohm et al., 2004; Vosper, 2004); (vi) channeling of valley winds due to the flow aloft (Whiteman and Doran, 1993). If a pressure gradient favourable to drive an across-mountain flow exists, the above processes may modify the local structure of the foehn. However, in this study, we consider the Puelche structure and evolution on a *regional* scale, rather than restricted to a single valley, for a period during which a Puelche foehn was observed near Lake Villarrica.

While the pioneering climatological analysis by Montecinos et al. (2017) points a way forward in the analysis of the Puelche foehn, it cannot be conclusive in some *regional* aspects of the Puelche foehn winds because of the still rather coarse resolution ($0.5° \times 0.5°$) of the used reanalysis dataset. In this study, we investigate the detailed regional structure and temporal evolution of a Puelche foehn event during 25–26 March 2014. More specifically, we address the following questions:

1. Which synoptic conditions lead to this particular Puelche foehn event?
2. What is the regional structure of the Puelche foehn winds, and how does the spatial and temporal evolution relate to the synoptic forcing?
3. What is the relative importance of *zonal* and *meridional* large-scale pressure gradients for the *easterly* winds during this specific Puelche event?
4. What is the vertical structure of the foehn and is the flow on the eastern side of the Andes orographically blocked or not?

While the first of these questions is addressed by analyzing meteorological fields from the operational analysis of the European Centre for Medium-Range Weather Forecasts (ECMWF; www.ecmwf.int), the other questions require higher spatial resolution. To this aim, simulations with the numerical weather prediction model COSMO (COnsortium for Small-Scale Modelling; Steppeler et al., 2003) are performed. With a grid spacing of 2.2 km, these simulations capture the regional structure (question 2) of the Puelche winds well, and hence allow for the temporal and spatial evolution to be studied. We would like to stress, however, that it is not our goal to understand the very local features of the Puelche winds and thus we refrain from analyzing the fine-scale structure of the foehn wind within distinct valleys or at specific locations in detail. High-resolution simulations (at ~ 100 m grid spacing) would be needed to examine these aspects (e.g., Chow et al., 2006). Correspondingly, question 3, relating the pressure gradients to the zonal winds, is addressed by means of Eulerian cross-sections of the pressure field. Finally, we investigate question 4 with both Eulerian and Lagrangian perspectives by considering cross-sections, the dimensionless mountain height, and computing kinematic backward trajectories. The Lagrangian framework, in particular, has become an invaluable tool improving the process understanding of foehn in recent years (see, e.g., Takane and Kusaka, 2011; Elvidge et al., 2015; Sprenger and Wernli, 2015; Elvidge and Renfrew, 2016; Miltenberger et al., 2016).

To our knowledge, this is the first study focusing on the mesoscale dynamics of the Puelche foehn and, hence, it complements the larger-scale study by Montecinos et al. (2017). The paper is structured as follows: In Section 2, the data and methods are explained. Then, in Section 3, the spatial and temporal evolution of the Puelche foehn event and the origin of the associated air parcels are investigated. Finally, the results are set into a broader context in the summary and conclusion in Section 4.

2 Data and methods

Operational ECMWF analyses are used to evaluate the synoptic weather conditions. The data have an equivalent horizontal resolution of ~ 16 km on a reduced Gaussian grid with 137 vertical levels and are available at 6-hourly intervals. For our purposes, they are interpolated in the horizontal onto a latitude-longitude grid with a resolution of 0.25°.

To realistically represent the mesoscale dynamics of this Puelche event, we perform simulations using the limited-area model COSMO (Steppeler et al., 2003) in a two-step nesting approach. The coarser COSMO-7 simulation is initialized at 00 UTC 24 March 2014 with the initial and boundary conditions provided by the ECMWF operational analyses. It has a horizontal grid spacing of 6.6 km and 40 vertical levels, and provides the initial and boundary conditions for the finer-scale COSMO-2 simulation which is initialized at 06 UTC 24 March with a horizontal grid spacing of 2.2 km and 60 vertical levels. The region our study focuses on is shown with COSMO topography in Fig. 1. For a detailed description of the physical parameterizations used in the COSMO model, refer to Doms et al. (2011). The boundary layer height is estimated in the model using a bulk Richardson number criterion (e.g., Seibert et al., 2000).

Temperature and relative humidity ground measurements are taken from the DGA (Dirección General de Aguas) real time automated station in Pucón (http://dgasatel.mop.cl/), and serve to validate the COSMO-2 simulation. The measurements are available at hourly intervals, with some time steps missing. No wind data are measured at this station. The measurements are compared to pseudo measurements from COSMO-2 taken from the spatially averaged nine surface level grid points closest to the coordinates of Lake Villarrica (39.25° S, 72.08° W). Their location is marked in Figure 1.

Furthermore, air parcel backward trajectories are calculated based on the COSMO-2 wind field (at a higher 15-min interval), using the Lagrangian analysis tool LAGRANTO (Wernli and Davies, 1997; Sprenger and Wernli, 2015). 126 trajectories are started at 160 m above the ground in a rectangle around Lake Villarrica

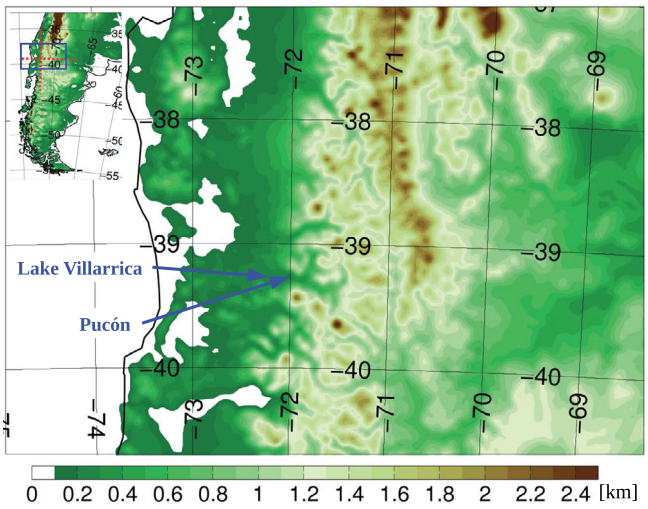

Figure 1: Region around Lake Villarrica with COSMO-2 topography (km, color shading). Its extent is indicated by the blue box in the subpanel depicting South America's COSMO-7 topography. The dashed red lines in the subpanel denote the location of the cross-sections in Figs. 4 and 7.

(within 72.07–72.3° W and 37.01–40.70° S) at different relevant time steps during this Puelche event and traced back in time for 24 h.

3 Results

On 25–26 March 2014, a strong Puelche event is recorded in Pucón during which near-surface temperature increases from 12 °C to 30 °C and relative humidity drops from above 90 % to below 20 % (Fig. 2a). These changes are smaller in the representative near-surface (at 10 m above the ground) model fields; but the onset time (06 UTC 25 March 2014; 03 local time) and the temporal evolution are captured remarkably well (Fig. 2b). In particular, the sharp increase (+3 °C) of simulated temperature at 03 local time associated with a sudden decrease in relative humidity cannot be related to the diurnal cycle since it occurs at night. Thus, it must be attributed to the Puelche's onset. Both, the model and the measurements show a short period of stagnation in the temperature increase before solar radiation sets in, and the foehn effect is no longer separable from the strong diurnal cycle. However, the COSMO-2 model's 2.2 km resolution limits its ability to simulate the local conditions at Pucón accurately because of the smoothed representation of topography (Fig. 1) and partly unresolved small-scale processes, including gravity waves, hydraulic jumps, mountain-valley circulation among others (see Section 1). Therefore, a direct comparison of the amplitude with point measurements is not meaningful, and we focus on the synoptic and regional scales in the following.

In the next section, the synoptic weather conditions associated with this specific Puelche event are examined based on ECMWF operational analyses. Then, the mesoscale structure, the driving mechanisms, and the origin of the foehn air parcels are investigated using Eulerian and Lagrangian diagnostics based on the COSMO-2 model data.

3.1 Synoptic weather conditions

On 24 March until the beginning of 25 March, a mid- and upper tropospheric ridge is located west of South America and a trough above the continent (shown in Figs. 3a, b at 500 hPa). During 25 March, a cut-off low forms north of the eastward propagating ridge, giving rise to easterly winds in the mid- and upper troposphere above Lake Villarrica (Fig. 3c). The cut-off low remains stationary until 00 UTC 27 March (Fig. 3d). In the lower troposphere, a persistent shallow coastal low develops north of Lake Villarrica on 25 March, which extends vertically from the surface to ~ 700 hPa (shown in Fig. 3b for 850 hPa), and advances further south (Figs. 3b, c) until it completely divides the zonal band of high geopotential height in the south (Fig. 3d). The geostrophic cyclonic flow around this coastal low is easterly near Lake Villarrica during the Puelche event. This synoptic configuration is consistent with the one found in the climatological analysis of Puelche events of Montecinos et al. (2017).

Even though the ECMWF operational analyses feature easterlies throughout the entire tropospheric column in the region of Lake Villarrica, the strong Puelche wind magnitude is not detected: The maximum wind speed in the lower troposphere never reaches 15 m s^{-1} and rarely exceedes 10 m s^{-1} in the first 200 m above the ground (not shown). Additionally, neither foehn effects in temperature nor in relative humidity are discernible in the ECMWF analyses (not shown). Hence, the synoptic environment is clearly favourable for a Puelche foehn, but the higher resolution of the COSMO-2 simulations is needed to capture the regional and temporal structure of the Puelche.

3.2 Spatio-temporal structure and driving mechanisms of the Puelche

The COSMO-2 model simulates strong near-surface Puelche winds over and in the lee of the Andes, which, in the lee, reach intensities of up to 24 m s^{-1} during the night of 26 March and extend meridionally over more than 400 km (Fig. 4). These maxima in near-surface wind speed are concomitant with the strongest easterlies in the mid- and upper troposphere. However, although easterlies prevail throughout the atmospheric column, the surface wind maxima are clearly separated from the wind maximum above 5000 m and there is no obvious link between them. While the zonal component of the mid- and upper tropospheric easterly winds is in geostrophic balance[2] (black contours in Fig. 4), this

[2]The computation of the zonal component of the geostrophic wind shown in Fig. 4 is described in Appendix A.

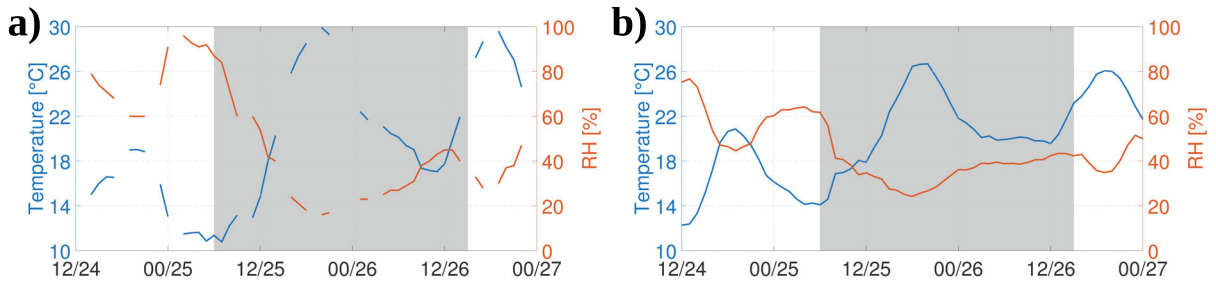

Figure 2: Time series of temperature (°C, blue line) and relative humidity (RH, %, orange line) of (a) in-situ measurements in Pucón and (b) the average over the nine COSMO-2 grid points closest to Lake Villarrica at the surface level at 10 m above the ground. The *x*-axes display UTC time in hours/day and the gray areas depict the time frame during which the model wind speed at the surface level exceeds 4 m s^{-1}. The discontinuities in panel a refer to missing data.

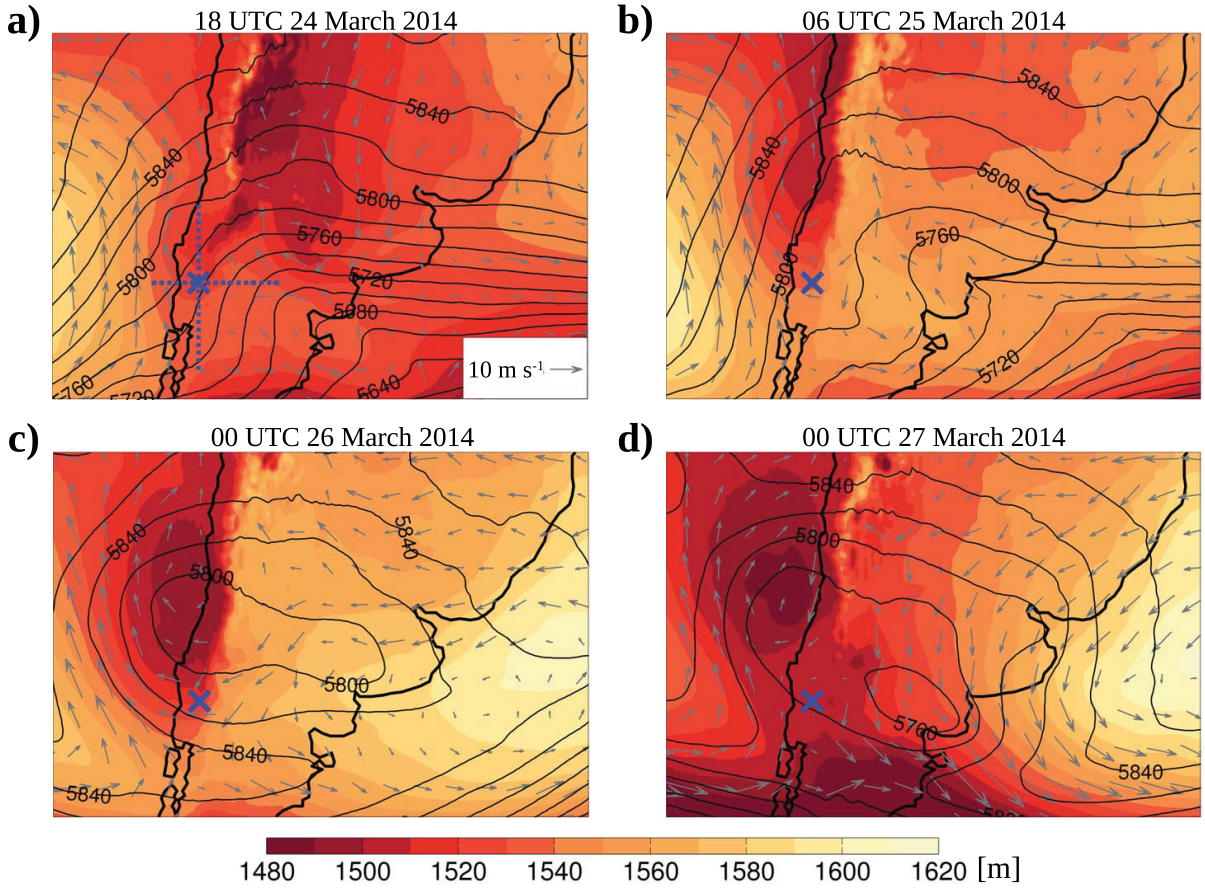

Figure 3: ECMWF analysis geopotential height at 500 hPa (m, black lines with a spacing of 20 m) and at 850 hPa (m, color). The gray arrows indicate the wind at 850 hPa and the blue cross marks Lake Villarrica's location. The dashed blue lines in panel a denote the location of the cross-sections in Figs. 4 and 7.

is not the case for the zonal winds closer to the surface: There, geostrophic balance would imply significantly weaker (maximum magnitude 14 m s^{-1}) zonal wind speeds; in particular, the fine-scale structure of the wind field near the surface is completely missed by the geostrophic winds.

Easterly near-surface winds first occur in the night of 24 March northeast of Lake Villarrica (Fig. 5a). Later, the Puelche winds set in near Lake Villarrica at 06 UTC 25 March (Fig. 5b), i.e., at the time when temperature and relative humidity show a distinct foehn signal in the COSMO pseudo measurements (Fig. 2b). During the next hours, the meridional and the zonal extent of the strong Puelche easterlies further increases until 13 UTC 25 March (10 local time, Fig. 5c). Afterwards, the easterly winds weaken for a short period (Fig. 5d), but intensify and reach peak intensity and extent in the night of 26 March (Fig. 5e). At 16 UTC 26 March, the easterlies have ceased to the north and at Lake Villarrica but are still weakly observable south of it (Fig. 5f).

West-east cross-sections at the latitude of Lake Villarrica (Fig. 6) give insight into the vertical structure of

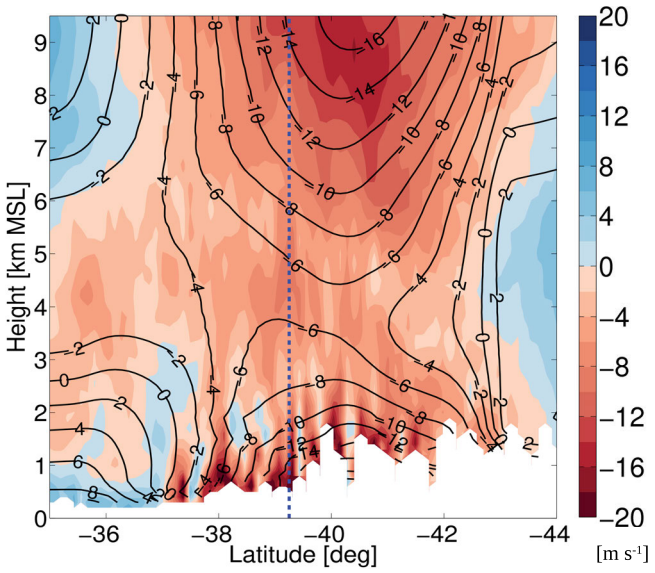

Figure 4: Vertical north-south cross-section of COSMO-2 zonal wind ($m\,s^{-1}$, color) dissecting Lake Villarrica at 00 UTC 26 March 2014. Additionally, the geostrophic wind ($m\,s^{-1}$, black lines with a spacing of $2\,m\,s^{-1}$) is shown. The dashed vertical blue line indicates Lake Villarrica's location and the covered region is marked by a dashed blue line in Fig. 3a and a dashed red line in Fig. 1.

the wind field. Before the start of the Puelche event, westerlies dominate near the surface over Lake Villarrica, while at higher levels, a band of weak easterlies is discernible (Fig. 6a). At 06 UTC 25 March, the decoupling of mid- and low-tropospheric flow disappears, and the easterlies extend down to the surface (Fig. 6b) concomitant with the observed foehn signatures above Lake Villarrica (Fig. 2b). As time progresses, the vertical and zonal extent of the strong easterlies increases in the early morning hours (Fig. 6c) before declining again (Fig. 6d). Then, in the night of 26 March, the strongest easterlies are observed which extend all the way to the coast (Fig. 6e). Finally, at 16 UTC 26 March, surface westerlies prevail again at Lake Villarrica, indicating the end of the Puelche foehn (Fig. 6f).

To better understand the large-scale driving mechanisms of the easterlies, and thus determine the respective importance of geostrophically balanced and cross-range-pressure-driven flow, we examine two levels, namely, 5000 m above sea level and 160 m above ground level. The evolution of *zonal* wind speed and pressure in the *zonal* and *meridional* directions are examined using Hovmöller diagrams and point values (Fig. 7).

As evident for the timing of peak easterlies (Fig. 4), the flow is geostrophically balanced in the free troposphere sufficiently far above the mountain range. Indeed, the evolution of the easterlies at 5000 m closely follows the evolution of the meridional large-scale pressure gradient force at this level (Fig. 7a). Specifically, at this height, the turning of the wind to easterlies coincides with a reversal in the meridional pressure gradient associated with the buildup of high pressure on the southern side. Although the deepening of the cut-off low on the northern side continues during 27 March, the meridional pressure gradient reverses again due to the weakening of the high-pressure anomaly to the south, and thus, weak westerlies ensue.

Next, we examine the formation of easterly winds near the surface and how they depend on the meridional and zonal components of the pressure gradient (Figs. 7b–e). To this aim, we consider the evolution of the surface pressure *anomaly*, which is computed as the deviation relative to the surface pressure at the time before the Puelche sets in (namely 12 UTC 24 March, marked with the dashed horizontal blue line in Figs. 7b, c). A meridional pressure gradient, responsible for the weak geostrophic component of the easterlies, is established initially (starting around 00 UTC 25 March) due to increasing pressure to the south and the subsequent deepening of the coastal low to the north (Figs. 3 and 7b, d). At this near-surface level, however, the zonal component of the pressure gradient developing across the ridge strongly exceeds the meridional one (Figs. 3 and 7c, d). Hence, easterlies develop around 00 UTC 25 March (Fig. 7e) in accordance with the increasing pressure on the eastern and southern side of the mountain range, and, later, enhanced by the pressure drop on the lee side associated with the coastal low (Figs. 7b, c). Thereby, the strongest easterlies, occurring around 00 UTC 26 March (Fig. 7e), coincide with the strongest meridional as well as zonal pressure gradients (Fig. 7d). Shortly after, the north-south gradient weakens while the easterly wind speed remains high which can be explained by the continuously strong east-west gradient (Figs. 7d, e). The reduction of pressure east of Lake Villarrica around 14 UTC 26 March is concurrent with the complete demise of the easterlies near the surface, even though the coastal low continues to intensify (Figs. 7c–e). Hence, ageostrophic flow associated with a cross-range pressure gradient is the dominant mechanism establishing near-surface easterlies. This analysis shows, however, that two transient features of the evolution of the easterlies cannot be attributed directly to the large-scale pressure gradient forces, namely the decrease in the intensity around 18 UTC 25 March, and the westerlies around 18 UTC 26 March (Fig. 7e), which may be caused by other, smaller-scale processes and linked to the daily cycle of thermally driven circulations.

3.3 Origin of the air parcels participating in the downslope winds

The absence of precipitation on the upstream side of the Andes implies that latent heat release does not play an important role for this Puelche event (not shown). Therefore, isolines of potential temperature approximate streamlines of the easterlies and the origin of the foehn air parcels can be estimated from the vertical structure of potential temperature (Fig. 6). During the Puelche event, the air is stably stratified on the eastern side of the Andes

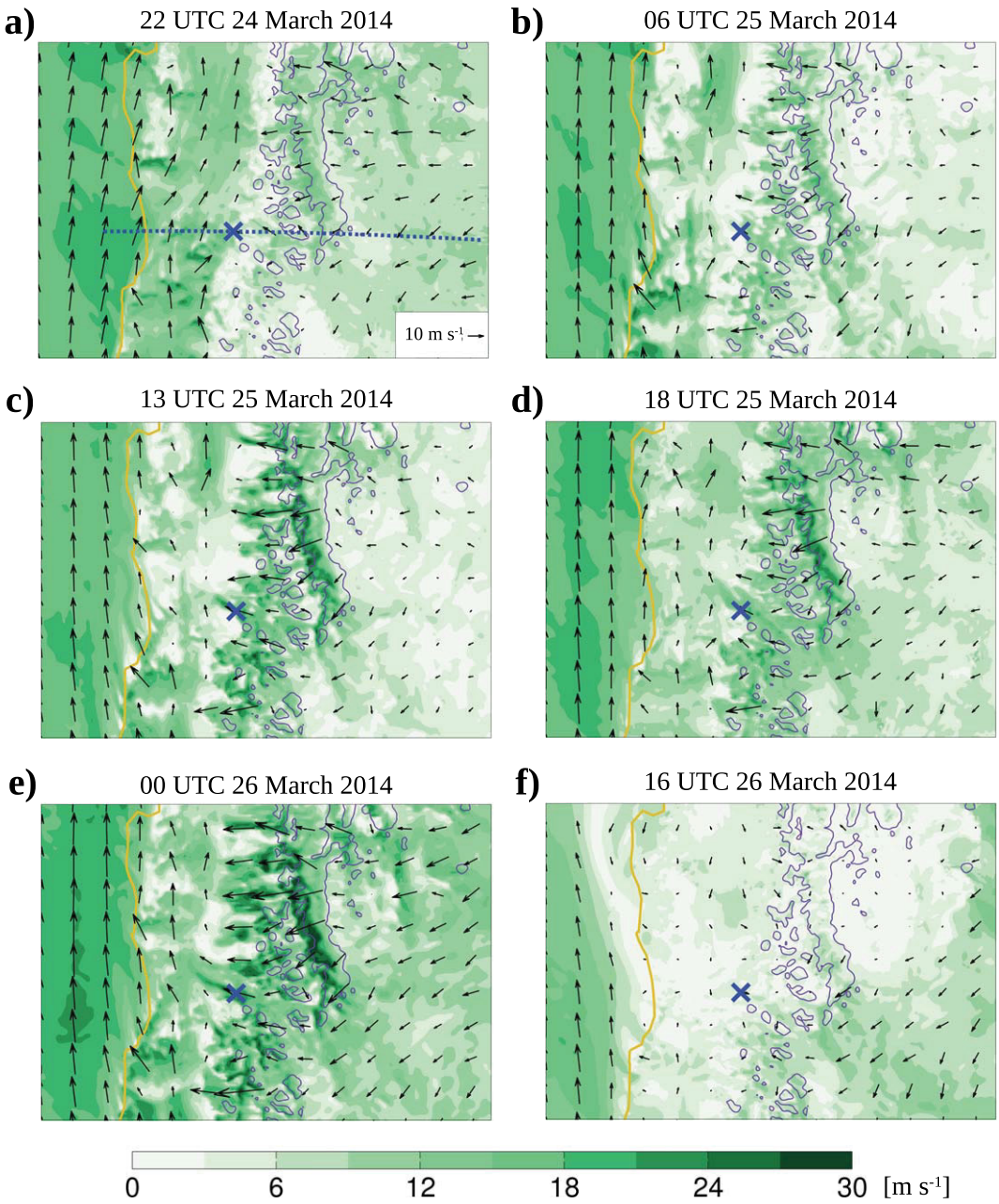

Figure 5: COSMO-2 wind speed (m s^{-1}, color) and the associated wind vectors (black) at 160 m above the ground. The golden line marks the coast and the purple line the 1500 m contour line of topography. Lake Villarrica's location is given by the blue cross and the covered region corresponds to the region shown in Fig. 1. The dashed blue line in panel a denotes the location of the vertical cross-sections in Fig. 6.

at nighttime (e.g., Fig. 6b), thereby preventing ascent to crest level. In contrast, a deep well-mixed boundary layer develops throughout the day, which, however, is still capped by an inversion located at about crest height (e.g., Fig. 6d). The presence of an inversion at or below crest level suggests that the Puelche air parcels originate from the mid-troposphere before they descend on the lee side of the Andes. Interestingly, however, easterlies, albeit weaker than at higher levels, are also present in the levels below the inversion (Figures 6c–e), indicating that some low-level air parcels may partake in the Puelche winds by flowing through gaps in the mountain range.

These arguments can be further extended by introducing the concept of a dimensionless mountain height (e.g., Reinecke and Durran, 2008) with which we can quantify whether the upstream environment is indicative of blocked, unblocked, or mixed foehn flow. The dimensionless mountain height, H^*, is given by $H^* = \frac{N \cdot H}{U}$, where N is the Brunt-Väisälä frequency, H the mountain height and U the upstream wind velocity. A systematic analysis is carried out for three locations upstream (4° east) of Lake Villarrica (indicated by the asterisks in Fig. 8a), at different times during the Puelche event. At each of the locations, H is the maximum topography height in the westward direction relative to the height of the upstream point. Because this height fluctuates strongly along single transects due to local peaks and gaps, the topography is meridionally averaged in a

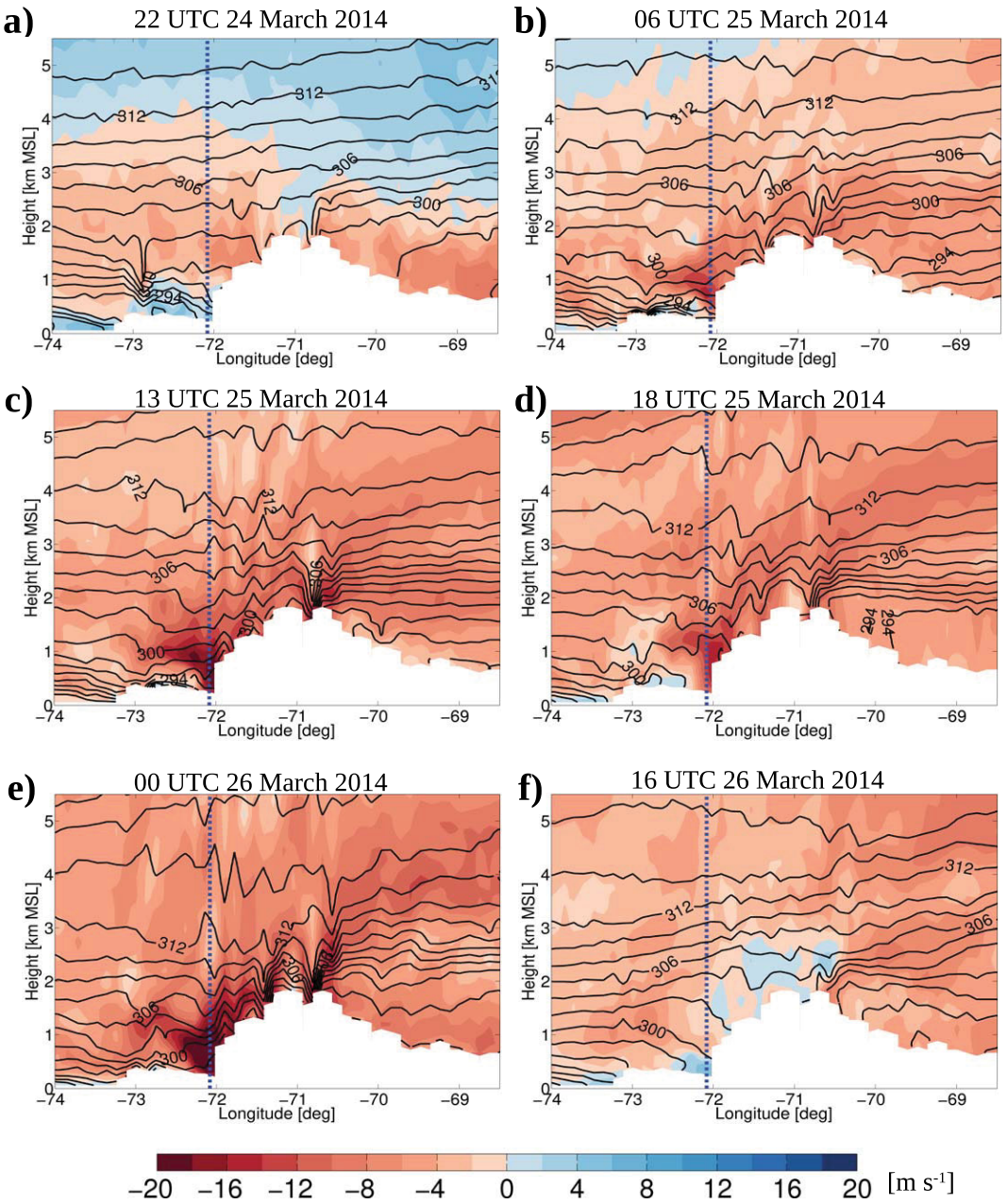

Figure 6: Vertical west-east cross-sections of COSMO-2 zonal wind speed (m s^{-1}, color) and potential temperature (K, black lines with a spacing of 2 K) dissecting Lake Villarrica. The dashed vertical blue line indicates Lake Villarrica's location and the covered region is marked by the dashed blue line in Fig. 5a.

band of 50 km width, as indicated by the dashed lines in Fig. 8a. The wind component in the westward direction at the upstream point is averaged in the layer below crest height and over the 50 km band width to obtain U. Finally, the Brunt-Väisälä frequency N is calculated using a bulk method (see e.g., Reinecke and Durran, 2008) as the square root of $N^2 = \frac{2 \cdot g}{(\theta_t + \theta_b)} \cdot \frac{(\theta_t - \theta_b)}{H}$, where θ_t and θ_b are the band-width-averaged potential temperatures at the crest height and the surface, respectively. The resulting H^* is highly variable in space and time but always > 1 and thus indicative of blocked easterly flow (Table 1). Between 12 UTC 25 March and 00 UTC 26 March, H^* decreases monotonously to the east and northeast of Lake Villarrica. In the southeast, a transient minimum is reached at 18 UTC 25 March.

To gain further dynamical insight, we investigate the latitude of Lake Villarrica (location A in Fig. 8a) at a specific time slot, namely 18 UTC 25 March, when $H^* = 2.5$ (Fig. 8). In this latitudinal band, easterlies dominate throughout most of the troposphere, while the northerly wind component is also non-negligible up to a height of ~3.5 km above sea level (Fig. 8b). According to the static stability profile, the top of the planetary boundary layer is above 2 km above sea level (Fig. 8c). The very stable layer at the top of the boundary layer (Fig. 8c) is associated with strong wind speed and a

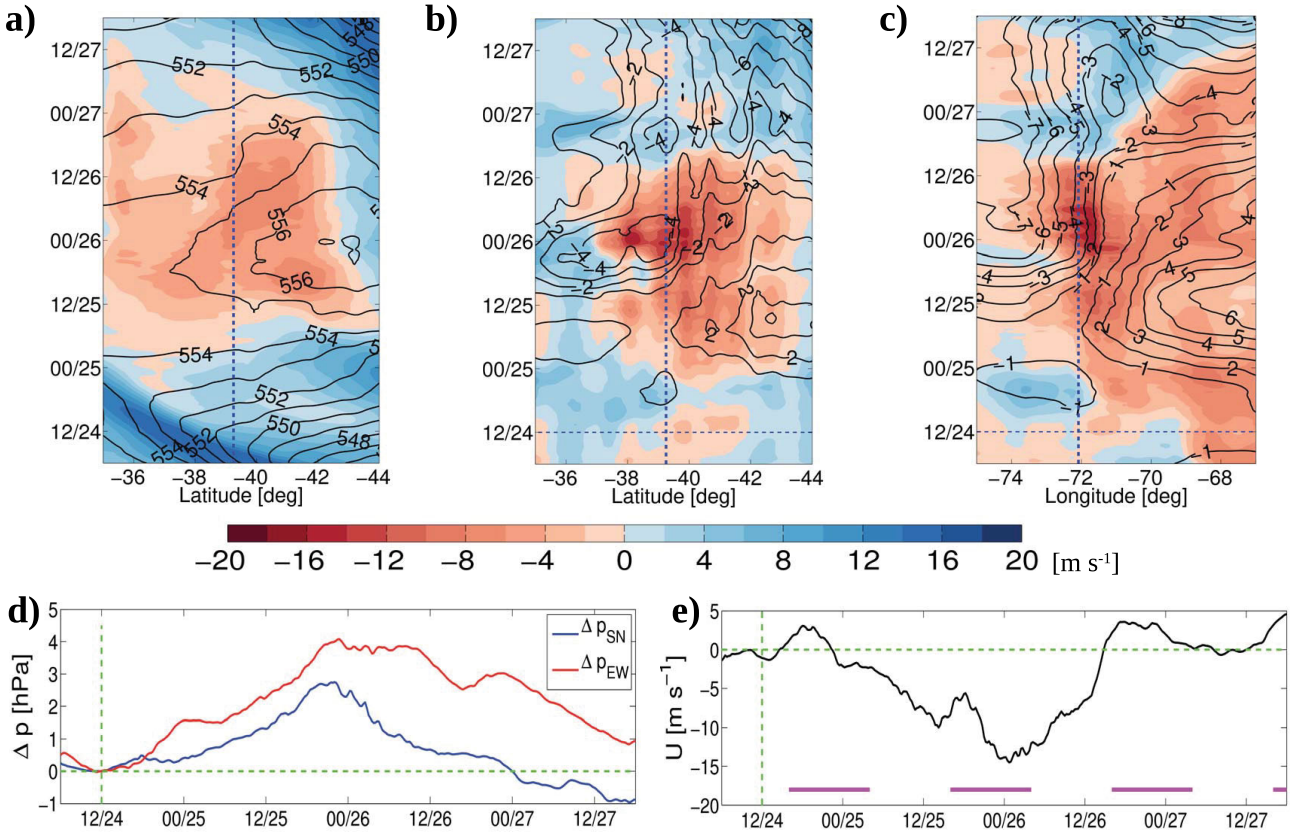

Figure 7: (a)–(c): Hovmöller diagrams dissecting Lake Villarrica showing COSMO-2 (a) zonal wind ($m\,s^{-1}$, color) and pressure (hPa, black lines with a spacing of 1 hPa) at 5000 m MSL in the north-south direction; (b) zonal wind ($m\,s^{-1}$, color) and pressure anomaly (hPa, black lines with a spacing of 1 hPa) at 160 m above ground in the north-south direction; (c) same as panel b but in the west-east direction. The *y*-axes display UTC time in hours/day. The pressure anomalies (panels b, c) are calculated as deviations relative to the pressure at 12 UTC 24 March 2014 (dashed horizontal blue lines). The dashed vertical blue lines indicate Lake Villarrica's location. The Hovmöller transects are marked by the dashed blue lines in Fig. 3a and the dashed red lines in Fig. 1. (d)–(e): Time series at 160 m above the surface of COSMO-2 (d) pressure difference relative to the pressure difference at 12 UTC 24 March 2014 taken over a distance of 1° in the meridional direction (p_{south}–p_{north}, blue line) and zonal direction (p_{east}–p_{west}, red line) centered at the position of Lake Villarrica (hPa) and (e) zonal wind speed ($m\,s^{-1}$, black line) at Lake Villarrica. The magenta lines indicate the nighttime periods (18–06 local time), the dashed vertical green lines the reference time to which pressure differences are calculated, and the dashed horizontal green lines the turning of the pressure gradient relative to the reference time (d) and the turning between westerlies and easterlies (e). The *x*-axes display UTC time in hours/day.

Table 1: Dimensionless mountain height, H^*, calculated for three upstream locations at different times. H is the averaged maximum relative mountain height (m) along the westward transects A–C, as indicated in Fig. 8a. The two numbers in brackets correspond to the averaged easterly wind component ($m\,s^{-1}$) and Brunt-Väisälä frequency (s^{-1}). See text for details on the determination of the parameters.

	SE of Villarrica (C) **40.25° S, 68.08° W** H **= 685 m**	**East of Villarrica (A)** **39.25° S, 68.08° W** H **= 1125 m**	**NE of Villarrica (B)** **37.25° S, 68.08° W** H **= 1625 m**
12 UTC 25 March	**5.1** ($2.0, 1.5 \cdot 10^{-2}$)	**3.0** ($5.7, 1.5 \cdot 10^{-2}$)	**9.5** ($2.3, 1.3 \cdot 10^{-2}$)
18 UTC 25 March	**1.3** ($3.0, 0.6 \cdot 10^{-2}$)	**2.5** ($3.3, 0.8 \cdot 10^{-2}$)	**4.5** ($3.9, 1.1 \cdot 10^{-2}$)
00 UTC 26 March	**1.6** ($3.6, 0.8 \cdot 10^{-2}$)	**1.9** ($5.4, 0.9 \cdot 10^{-2}$)	**4.0** ($5.1, 1.2 \cdot 10^{-2}$)

decoupling between the high- and low-level winds can be observed (Fig. 8b). The boundary layer surpasses the mountain barrier on the upstream side of the Andes along the transect (Fig. 8d). Thus, it should be possible for the air mass within the boundary layer close to the barrier to be advected over it with the low-level easterlies. This is in contradiction with the value of H^* of 2.5 (Table 1) indicating blocked flow. However, it needs to be emphasized that H^* does not take into account the detailed structure of the profiles of wind and Brunt-Väisälä frequency and is sensitive to the methodology it is computed with, potentially leading to misleading results. The bulk method H^* is calculated with the values: $U = 3.3\,m\,s^{-1}$, $N = 0.8 \cdot 10^{-2}\,s^{-1}$. If the averaging method is used instead, the values become $U = 3.3\,m\,s^{-1}$, $N = 0.6 \cdot 10^{-2}\,s^{-1}$, $H^* = 2.0$. Finally, one might take the values at mid-crest level and get $U = 3.2\,m\,s^{-1}$, $N = 0.4 \cdot 10^{-2}\,s^{-1}$, $H^* = 1.4$. In con-

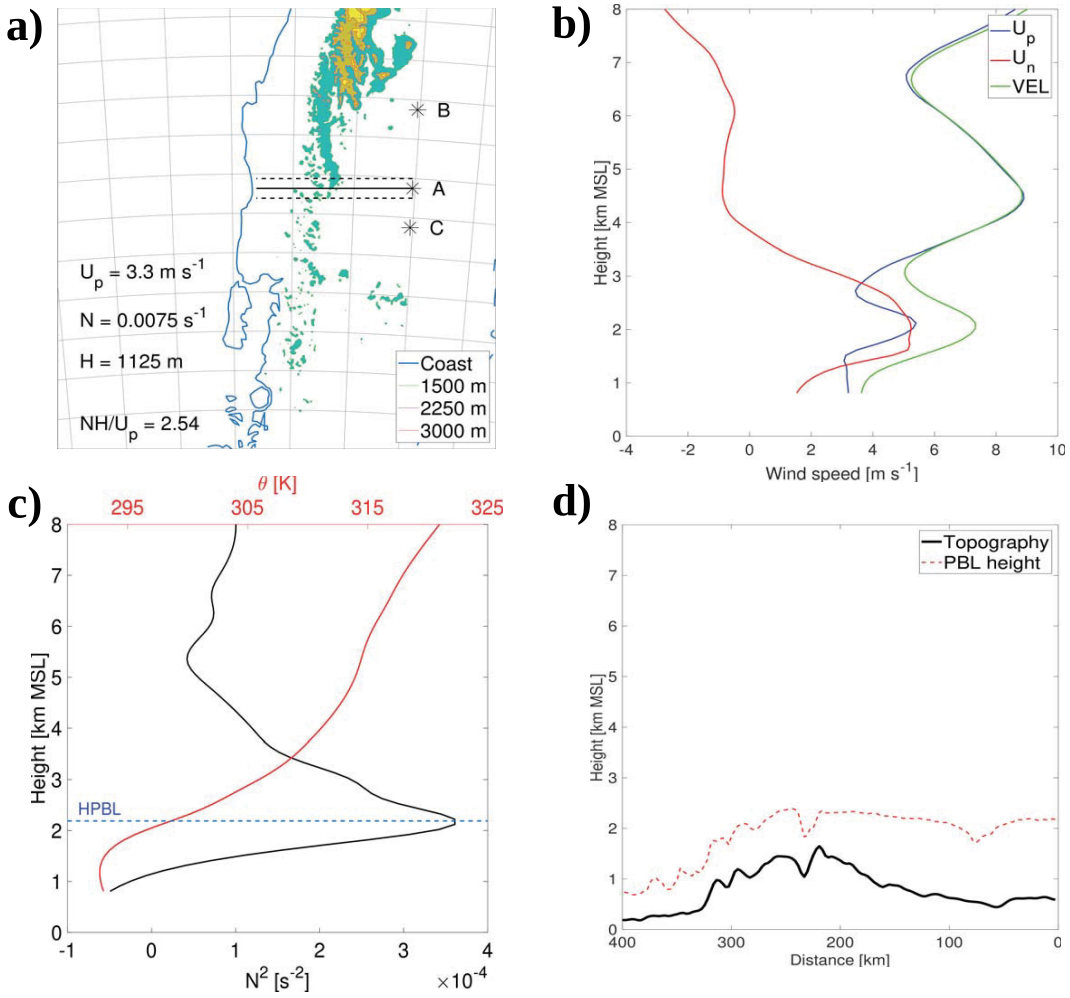

Figure 8: COSMO-2 parameters related to the dimensionless mountain height at 39.25° S, 68.08° W (asterisk A in panel a) at 18 UTC 25 March 2014: (a) Map view of model topography (m, color) and the locations where the dimensionless mountain height, H^*, is calculated (asterisks). While all three locations are used to determine H^* in Table 1, the parameters in this figure all relate to asterisk A and are averaged over the band covered by the dashed black lines. (b) Vertical profiles of the parallel (U_p, m s^{-1}, blue line) and normal (U_m, m s^{-1}, red line) wind components with respect to the black line orientation in panel a, and of the full velocity (VEL, m s^{-1}, green line). (c) Vertical profiles of potential temperature (θ, K, red line) and squared Brunt-Väisälä frequency (N^2, s^{-2}, black line). (d) Height of topography (km, black line) and planetary boundary layer above sea level (km, dashed red line), as a function of distance away from the upstream location (asterisk A) along the black line marked in panel a.

clusion, the estimates of H^* must be taken with some care.

At this time, similar conditions occur 1° south of Lake Villarrica (Table 1; location C in Fig. 8a). To the north (location B), although the upstream boundary layer height is around 2000 m (not shown), the flow is blocked more effectively by the higher mountain barrier and H^* is even higher (Table 1). The upstream boundary layer height is subject to a strong diurnal cycle and, consistent with the blocked flow conditions, often does not reach the crest height. It needs to be noted that the boundary layer height is taken as a direct model output which has to be treated with care, especially over complex topography. However, here, only the qualitative state of the boundary layer on the upstream side of the mountain range is examined. Hence, the modelled boundary layer height is a suitable indicator for our purpose.

A complementary view can be provided by the Lagrangian perspective, offering a comprehensive understanding of the Puelche wind by taking into account the realistic spatio-temporal variations of the flow field. Backward trajectories are initiated at six different times (as in Figs. 5 and 6) from the locations indicated by the black points in Fig. 9 from a height of 160 m above the ground. At 22 UTC 24 March (Fig. 9a), the air on the western side of the mountain range has not previously crossed the Andes, but instead originates from further south. During the night, easterlies develop over the mountain range (Figs. 5 and 6), and air parcels arriving at 06 UTC 25 March originate partially from the eastern side (Fig. 9b). The subsequent strengthening of the easterlies over the Andes (Figs. 5 and 6) implies that virtually all air parcels on the lee side have previously crossed the mountain range and thus, participate in the foehn flow (Fig. 9c).

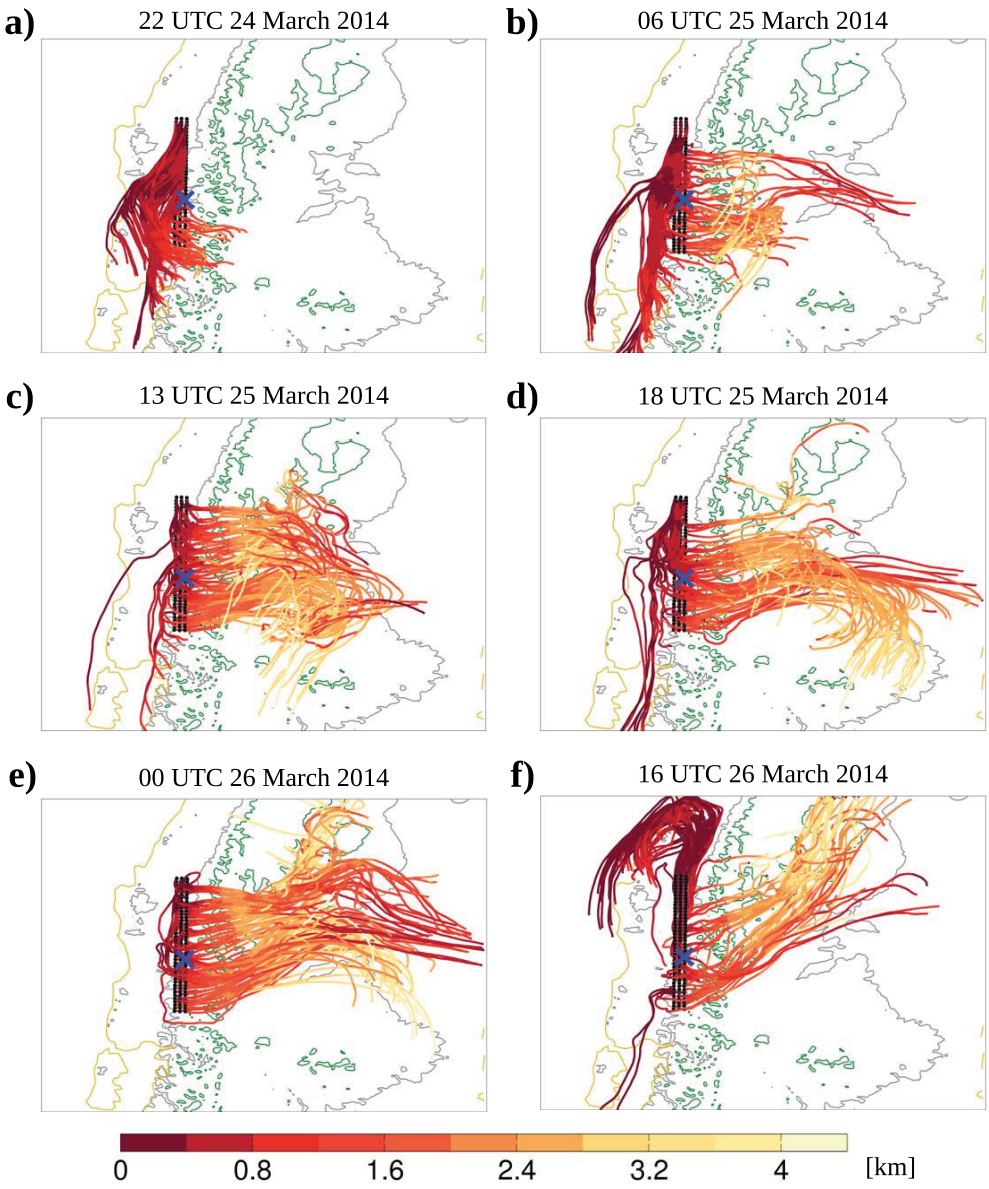

Figure 9: COSMO-2 backward trajectories from a region impacted by the Puelche foehn at 160 m above the ground, marked by the black dots. The trajectories are colored according to their height above sea level (km). The golden contour line depicts the coast, gray and green denote an elevation of 500 m and 1500 m respectively. The blue cross marks Lake Villarrica's location. The air parcel trajectories are started at the time indicated at each panel and run backwards in time for 24 h. Except for panel a and b where they are run back only until 12 UTC 24 March 2014 to account for the spin-up time of the model.

Air parcels arriving at 13 UTC 25 March to the north of Lake Villarrica originate from low altitudes, while air arriving south of Lake Villarrica originates largely from the Andes crest level above the inversion layer (Fig. 9c). This is interesting because the mountain barrier is higher in the north compared to the south. Still, the trajectories indicate non-blocked flow in the north while the southern air mass originates from higher up and turns from southerly to easterly before descending on the lee side. Note that the dimensionless mountain height H^* northeast of Lake Villarica (Table 1), in contrast, points towards blocked flow throughout the event (see next paragraph for a critical discussion). The transient weakening of the easterlies at 18 UTC 25 March (Figs. 5d and 6d), especially to the south of Lake Villarrica, is particularly concurrent with air originating from low levels and crossing the Andes through mountain gaps (Fig. 9d). Air parcels originating from both mid-tropospheric (4000 m) and near-surface levels, are also discernible at the time of maximum wind speed (Fig. 9e). Hence, non-blocked, and therefore, upslope flow is possible on the Andes eastern side, with the air being channeled through mountain gaps.

While both the Lagrangian and the Eulerian perspectives indicate that mixed blocked and non-blocked flow co-exists during this Puelche event, the Lagrangian approach captures the complex nature of the foehn flow in more detail. For instance, H^* always clearly exceeds 1 at the location northeast of Lake Villarrica but the trajectories reveal that nevertheless, some air parcels originate

from the lower troposphere there. Since the Lagrangian perspective follows individual air parcels it can take into account changes in the vertical stability – and thus also in H^* – connected to the diurnal cycle the air parcel experiences along its way. Hence, a deeper understanding of the origin of the air parcels participating in the foehn event can be gained by the inherent consideration of the complex flow evolution in the Lagrangian approach.

4 Summary and conclusion

In this numerical modelling study, we examined regional aspects of the dynamics of a Puelche event observed on 25–26 March 2014 near Lake Villarrica – a region in the southern Andes where only sparse observations are available. The COSMO-2 model successfully captures the Puelche event and yields novel dynamical insights into the structure and driving mechanisms of foehn winds in this region. In the following we summarize the main results in light of the questions posed in Section 1:

1. At the beginning of the Puelche event, a mid-tropospheric ridge is present west of the subtropical Andes and a trough over land. In the lower troposphere, a narrow coastal low forms along the western coast of South America with its tip reaching as far south as Lake Villarrica while the pressure increases on the eastern side of the Andes. Further south, high pressure dominates on both sides of the mountain range. In the mid- and upper levels, a cut-off low develops north of the eastward propagating ridge above the continent.

2. The easterly Puelche winds occur above the Andes and manifest as elongated jets of increased wind speeds along valleys on the lee side. Low-level easterlies exceeding 18 m s^{-1} extend over 400 km along, and 100 km across the mountain range. The event lasts about 32 h, which is a common lifetime of Puelche winds (Montecinos et al., 2017). Its duration is governed by the intensification and later the decay of the high-pressure system south and east of the mountain range, while the coastal low and the upper level cut-off low contribute as well.

3. Flow along isohypses in geostrophic balance is the key factor in explaining the easterly wind throughout the free troposphere. But within the planetary boundary layer, where frictional dissipation is strong, flow is also driven by large-scale cross-mountain pressure gradients – potentially enhanced by mesoscale processes, e.g., gravity waves and/or lee side subsidence and cyclogenesis. The easterly flow, initially in geostrophic balance upstream of the orographic barrier, is disturbed from geostrophy while crossing the barrier. The length scale required for the flow on the lee side to return to balanced conditions can be estimated as $\frac{u}{f}$, where u is the zonal wind speed, $\sim$ O(10 m s^{-1}), and f is the Coriolis parameter, $\sim$ O(10^{-4} s^{-1}), i.e., resulting in $\sim$ 100 km. The proximity of Lake Villarrica to the barrier, considerably below this length scale, implies that in this region, the easterlies which depart from geostrophy, cannot yet be adjusted back to geostrophic balance. Indeed, as demonstrated in detail in this study, the near-surface easterlies are to a large extent ageostrophic in nature.

4. This Puelche event can be classified as a mixed blocked and non-blocked foehn type. According to combined Eulerian and Lagrangian analyses, many air parcels arrive from above the capping inversion around crest height on the eastern side of the Andes, hence, indicative of blocked foehn. Nevertheless, some air parcels originate from the lowermost troposphere east of the Andes and are channeled through gaps in the mountain range. Furthermore, the event can be regarded as a deep foehn since the turning of the wind vectors with height is negligible, and easterlies span throughout the entire tropospheric column.

This study provides a first detailed numerical simulation of a Puelche event, in a region where the sparse observational network limits the inclusion of such cases as an integral component of mountain meteorology research. It remains an open question whether thermally driven circulations modulate the easterlies. For Raco cases, Rutllant and Garreaud (2004) suggest that under clear sky conditions, the strongest easterly wind anomalies occur preferably during night and in the early mornings which is also observed in this Puelche event. Additionally, smaller-scale processes affect the dynamics of the Puelche winds, which are yet to be studied using high-resolution modelling strategies in this region. Specifically, it would be interesting to explore how the Puelche is affected by the development of an inversion layer upstream of the mountain range and the associated lee waves.

Appendix A

The geostrophic wind, U_g, in Fig. 4 is calculated according to $U_g = \frac{R \cdot T}{f \cdot p} \cdot \frac{\partial p}{\partial y}$ where $f = 2 \cdot \Omega \cdot \sin(\phi)$ is the Coriolis parameter at Lake Villarrica's latitude $\phi = 39.25°$ S, T the temperature, p the pressure and, correspondingly, $\frac{\partial p}{\partial y}$ the meridional pressure gradient at a given height, as well as $\Omega = 7.29 \cdot 10^{-5}$ s^{-1} the Earth angular velocity, and $R = 287.05$ J kg^{-1} K^{-1} the specific gas constant of dry air. To obtain the vertical cross-section of U_g in Fig. 4, we interpolate the COSMO fields to a stack of height levels from the surface up to 10 km, in steps of 100 m. The pressure gradient is approximated by a meridional pressure difference across 12 grid points, centered at Lake Villarrica, and corresponding to a distance of 26.4 km.

In the non-hydrostatic COSMO model, the pressure field on a specific height level exhibits many small-scale spatial variations, e.g., due to gravity waves. Hence, we smooth pressure and temperature with a 40-point moving average in the meridional direction prior to computing the geostrophic wind. Accordingly, the geostrophic winds shown in Fig. 4 do not reflect the small-scale variations in the pressure fields, particularly at near-surface levels. Instead, they characterize the zonal wind speed resulting from the large-scale pressure field.

Acknowledgments

We would like to thank Francisca Muñoz for pointing us towards the DGA automated station data and the Ministerio de Obras Públicas for providing them. Additionally, we are thankful to MeteoSwiss for giving us access to the ECMWF data. Lukas Papritz acknowledges support by the Swiss National Science Foundation, grant P2EZP2_162267. Shira Raveh-Rubin is funded by the Swiss National Science Foundation Marie Heim-Voegtlin Programme (PMPDP2_158347/1). We thank the two anonymous reviewers and the editor for their comments on a previous version of the manuscript which helped to significantly improve the clarity of the paper.

References

Brinkmann, W.A.R., 1971: What is a Foehn? – Weather **26**, 230–240. DOI:10.1002/j.1477-8696.1971.tb04200.x.

Brock, B.W., F. Burger, A. Rivera, A. Montecinos, 2012: A fifty year record of winter glacier melt events in southern Chile, 38°–42° S. – Env. Res. Lett. **7**, 045403. DOI: 10.1088/1748-9326/7/4/045403.

Chow, F., A. Weigel, R. Street, M. Rotach, M. Xue, 2006: High-Resolution Large-Eddy Simulations of Flow in a Steep Alpine Valley. Part I: Methodology, Verification, and Sensitivity Experiments. – J. Appl. Meteor. Climatol. **45**, 63–86, DOI: 10.1175/JAM2322.1.

Colle, B.A., C.F. Mass, 1998: Windstorms along the Western Side of the Washington Cascade Mountains. Part I: A High-Resolution Observational and Modeling Study of the 12 February 1995 Event. – Mon. Wea. Rev. **126**, 28–52. DOI: 10.1175/1520-0493(1998)126<0028:watwso>2.0.co;2.

Doms, G., J. Förstner, E. Heise, H.-J. Herzog, D. Mironov, M. Raschendorfer, T. Reinhardt, B. Ritter, R. Schrodin, J.-P. Schulz, G. Vogel, 2011: A description of the nonhydrostatic regional COSMO model. Part II: Physical parameterization. – Consortium for Small-Scale Modelling Technical Report LM_F90 4.20, 154 pp. – Online available: www.cosmo-model.org/content/model/documentation/core/cosmoPhysParamtr.pdf (accessed at 15 August 2017).

Drobinski, P., R. Steinacker, H. Richner, K. Baumann-Stanzer, G. Beffrey, B. Benech, H. Berger, B. Chimani, A. Dabas, M. Dorninger, B. Dürr, C. Flamant, M. Frioud, M. Furger, I. Gröhn, S. Gubser, T. Gutermann, C. Häberli, E. Häller-Scharnhost, G. Jaubert, M. Lothon, V. Mitev, U. Pechinger, M. Piringer, M. Ratheiser, D. Ruffieux, G. Seiz, M. Spatzierer, S. Tschannett, S. Vogt, R. Werner, G. Zängl, 2007: Föhn in the Rhine Valley during MAP: A review of its multiscale dynamics in complex valley geometry. – Quart. J. Roy. Meteor. Soc. **133**, 897–916. DOI:10.1002/qj.70.

Durran, D.R., 1990: Mountain waves and downslope winds. – In: Blumen, W. (Ed.): Atmospheric processes over complex terrain. – Amer. Meteor. Soc., 59–81. DOI: 10.1007/978-1-935704-25-6.

Elvidge, A.D., I.A. Renfrew, 2016: The Causes of Foehn Warming in the Lee of Mountains. – Bull. Amer. Meteor. Soc. **97**, 455–466, DOI:10.1175/BAMS-D-14-00194.1.

Elvidge, A.D., I.A. Renfrew, J.C. King, A. Orr, T.A. Lachlan-Cope, M. Weeks, S.L. Gray, 2015: Foehn jets over the Larsen C Ice Shelf, Antarctica. – Quart. J. Roy. Meteor. Soc. **141**, 698–713. DOI:10.1002/qj.2382.

Garreaud, R.D., 2009: The Andes climate and weather. – Adv. Geosci. **22**, 3–11. DOI:10.5194/adgeo-22-3-2009.

Garreaud, R.D., J.A. Rutllant, H. Fuenzalida, 2002: Coastal Lows along the Subtropical West Coast of South America: Mean Structure and Evolution. – Mon. Wea. Rev. **130**, 75–88. DOI:10.1175/1520-0493(2002)130<0075:clatsw>2.0.co;2.

Gohm, A., G.J. Mayr, 2004: Hydraulic aspects of föhn winds in an Alpine valley. – Quart. J. Roy. Meteor. Soc. **130**, 449–480. DOI:10.1256/qj.03.28.

Gohm, A., G. Zängl, G.J. Mayr, 2004: South Foehn in the Wipp Valley on 24 October 1999 (MAP IOP 10): Verification of High-Resolution Numerical Simulations with Observations. – Mon. Wea. Rev. **132**, 78–102. DOI:10.1175/1520-0493(2004)132<0078:SFITWV>2.0.CO;2.

Hann, J., 1866: Zur Frage über den Ursprung des Föhns. – Zeitschrift der Österreichischen Gesellschaft für Meteorologie **1**, 257–263.

Hobbs, J.E., J.A. Lindesay, H.A. Bridgman, 1998: Climates of the southern continents. Present, Past and Future. – John Wiley & Sons, 318 pp.

Klemp, J., D. Lilly, 1975: The Dynamics of Wave-Induced Downslope Winds. – J. Atmos. Sci. **32**, 320–339. DOI: 10.1175/1520-0469(1975)032<0320:TDOWID>2.0.CO;2.

Kuhn, M., 1989: Föhnstudien. – Wissenschaftliche Buchgesellschaft Darmstadt, 504 pp.

Mayr, G.J., L. Armi, A. Gohm, G. Zängl, D.R. Durran, C. Flamant, S. Gaberšek, S. Mobbs, A. Ross, M. Weissmann, 2007: Gap flows: Results from the Mesoscale Alpine Programme. – Quart. J. Roy. Meteor. Soc. **133**, 881–896. DOI: 10.1002/qj.66.

Meruane, C., Y. Niño, R.D. Garreaud, 2006: Response of the thermal structure of Lake Villarrica (Chile) to strong, foehn-like winds: Field study and numerical simulations. – Technical Report. Online available: carolina.meruane.com/wp-content/uploads/2012/04/cmeruaneetal_2006.pdf (accessed at 15 August 2017).

Miltenberger, A.K., S. Reynolds, M. Sprenger, 2016: Revisiting the latent heating contribution to foehn warming – Lagrangian analysis of two foehn events over the Swiss Alps. – Quart. J. Roy. Meteor. Soc. **142**, 2194–2204. DOI: 10.1002/qj.2816.

Montecinos, A., R.C. Muñoz, S. Oviedo, A. Martínez, V. Villagrán, 2017: Climatological characterization of Puelche winds down the western slope of the extratropical Andes Mountains using the NCEP Climate Forecast System Reanalysis. – J. Appl. Meteor. Climatol. DOI:10.1175/JAMC-D-16-0289.1.

Montes, C., J.A. Rutllant, A. Aguirre, L. Bascuñán-Godoy, C. Juliá, 2016: Terral de Vicuña, a Foehnlike Wind in Semiarid Northern Chile: Meteorological Aspects and Implications for the Fulfillment of Chill Requirements in Deciduous Fruit Trees. – J. Appl. Meteor. Climatol. **55**, 1183–1196. DOI: 10.1175/JAMC-D-15-0275.1.

Nkemdirim, L.C., 1996: Canada's chinook belt. – Int. J. Climatol. **16**, 441–462. DOI:10.1002/(SICI)1097-0088(199604)16:4<441::AID-JOC21>3.0.CO;2-T.

Reinecke, P.A., D.R. Durran, 2008: Estimating topographic blocking using a Froude number when the static stability is nonuniform. – J. Atmos. Sci. **65**, 1035–1048. DOI:10.1175/2007JAS2100.1.

Richner, H., P. Hächler, 2013: Understanding and Forecasting Alpine Foehn. – In: Chow, F., S. De Wekker, B. Snyder (Eds.): Mountain Weather Research and Forecasting. – Springer Atmospheric Sciences **4**, 219–260. DOI:10.1007/978-94-007-4098-3_4.

Rutllant, J.A., R.D. Garreaud, 2004: Episodes of strong flow down the western slope of the subtropical Andes. – Mon. Wea. Rev. **132**, 611–622. DOI:10.1175/1520-0493(2004)132<0611:EOSFDT>2.0.CO;2.

Seibert, P., 1990: South Foehn Studies since the ALPEX Experiment. – Meteor. Atmos. Phys. **43**, 91–103, DOI:10.1007/bf01028112.

Seibert, P., F. Beyrich, S.-E. Gryning, S. Joffre, A. Rasmussen, P. Tercier, 2000: Review and intercomparison of operational methods for the determination of the mixing height. – Atmos. Env. **34**, 1001–1027. DOI:10.1016/S1352-2310(99)00349-0.

Seluchi, M.E., F.A. Norte, P. Satyamurty, S.C. Chou, 2003: Analysis of Three Situations of the Foehn Effect over the Andes (Zonda Wind) using the Eta-CPTEC Regional Model. – Wea. Forecast. **18**, 481–501. DOI:10.1175/1520-0434(2003)18<481:AOTSOT>2.0.CO;2.

Sprenger, M., C. Schär, 2001: Rotational aspects of stratified gap flows and shallow foehn. – Quart. J. Roy. Meteor. Soc. **127**, 161–187. DOI:10.1002/qj.49712757110.

Sprenger, M., H. Wernli, 2015: The LAGRANTO Lagrangian analysis tool – version 2.0. – Geosci. Model Develop. **8**, 2569–2586. DOI:10.5194/gmd-8-2569-2015.

Sprenger, M., O. Martius, J. Arnold, 2013: Cold surge episodes over southeastern Brazil – a potential vorticity perspective. – Int. J. Climatol. **33**, 2758–2767. DOI:10.1002/joc.3618.

Sprenger, M., B. Dürr, H. Richner, 2016: Foehn Studies in Switzerland. – In: Willemse, S., M. Furger (Eds.): From weather observations to atmospheric and climate sciences in Switzerland: Celebrating 100 years of the Swiss Society for Meteorology. – Online available: vdf.ch/from-weather-observations-to-atmospheric-and-climate-sciences-in-switzerland-e-book.html (accessed at 15 August 2017).

Steppeler, J., G. Doms, U. Schättler, H.W. Bitzer, A. Gassmann, U. Damrath, G. Gregoric, 2003: Meso-gamma scale forecasts using the nonhydrostatic model LM. – Meteor. Atmos. Phys. **82**, 75–96. DOI:10.1007/s00703-001-0592-9.

Takane, Y, H. Kusaka, 2011: Formation Mechanisms of the Extreme High Surface Air Temperature of 40.9 °C observed in the Tokyo Metropolitan Area: Considerations of Dynamic Foehn and Foehnlike Wind. – J. Appl. Meteor. Climatol. **50**, 1827–1841, DOI:10.1175/JAMC-D-10-05032.1.

Vosper, S.B., 2004: Inversion effects on mountain lee waves. – Quart. J. Roy. Meteor. Soc. **130**, 1723–1748. DOI:10.1256/qj.03.63.

Wernli, H., H.C. Davies, 1997: A Lagrangian-based analysis of extratropical cyclones. I: The method and some applications. – Quart. J. Roy. Meteor. Soc. **123**, 467–489. DOI:10.1002/qj.49712353811.

Wuersch, M., M. Sprenger, 2015: Swiss and Austrian Foehn revisited: A Lagrangian-based analysis. – Meteorol. Z. **24**, 225–242. DOI:10.1127/metz/2015/0647.

Whiteman, C., J. Doran, 1993: The Relationship between Overlying Synoptic-Scale Flows and Winds within a Valley. – J. Appl. Meteor. **32**, 1669–1682, DOI:10.1175/1520-0450(1993)032<1669:TRBOSS>2.0.CO;2.